Available online at www.sciencedirect.com
ScienceDirect
Trans. Nonferrous Met. Soc. China 30(2020) 382−391
Transactions of Nonferrous Metals Society of China
www.tnmsc.cn

Microstructures and properties of porous TiAl-based intermetallics prepared by freeze-casting

Zhong-liang LU[1,2,3], Wen-liang XU[1], Ji-wei CAO[1], Yuan-lin XIA[1], Qing-hua DENG[4], Di-chen LI[1]

1. State Key Laboratory for Manufacturing Systems Engineering, School of Mechanical Engineering, Xi'an Jiaotong University, Xi'an 710049, China;
2. State Key Laboratory of Light Alloy Casting Technology for High-end Equipment, Shenyang Research Institute of Foundry, Shenyang 110022, China;
3. Collaborative Innovation Center for Advanced Aero-Engine, Beijing 100191, China;
4. School of Energy and Power Engineering, Xi'an Jiaotong University, Xi'an 710049, China

Received 8 June 2019; accepted 12 November 2019

Abstract: Preparation of porous TiAl-based intermetallics with aligned and elongated pores by freeze-casting was investigated. Engineering Ti−43Al−9V−1Y powder (D_{50}=50 μm), carboxymethyl cellulose, and guar gum were used to prepare the aqueous-based slurries for freeze-casting. Results showed that the porous TiAl was obtained by using a freezing temperature of −5 °C and the pore structure was tailored by varying the particle content of slurry. The total porosity reduced from 81% to 62% and the aligned pore width dropped from approximately 500 to around 270 μm, with increasing the particle content from 10 to 30 vol.%. Furthermore, the compressive strength along the aligned pores increased from 16 to 120 MPa with the reduction of porosity. The effective thermal conductivities of porous TiAl were lower than 1.81 W/(m·K) and showed anisotropic property with respect to the pore orientation.
Key words: porous TiAl; freeze-casting; pore structures; mechanical properties; thermal conductivity

1 Introduction

TiAl-based alloys have been considered as one of the most promising high temperature structural materials due to their light weight, high specific strength, as well as good environmental resistance at elevated temperature [1−4]. In order to further explore the potential industrial application of TiAl, efforts have been made to produce TiAl materials with tailored porous structure, which are expected to be applied in the fields such as lightweight structure, filtering, and thermal insulation [5−7]. Currently, various processes have been developed to yield porous TiAl. The element powder metallurgy (EPM) has been widely investigated to produce porous TiAl with utilization of the Kirkendall effect [5,8,9]. However, the porosity of the material fabricated with this process is generally limited. To directly control the porosity in the synthesis of porous TiAl, the space holder method has been developed. Under the Kirkendall effect and replication of space holders, highly porous TiAl with bimodal isotropic pore structure and various porosities could be obtained [10,11]. Some other processes were also proposed to fabricate highly open cellular porous TiAl, including thermal explosion (TE) [12] and spark plasma sintering (SPS) [13].

Recently, the fabrication of porous metal materials with aligned pore structures has become a fascinating subject. Reactive sintering of extruded

Foundation item: Projects (51775418, 51375372) supported by the National Natural Science Foundation of China
Corresponding author: Di-chen LI, Tel: +86-29-82665126, E-mail: xjtudcli@sina.com; Zhong-liang LU, E-mail: zllu@mail.xjtu.edu.cn
DOI: 10.1016/S1003-6326(20)65220-7

powder mixtures was applied to fabricating aligned porous TiAl−Mn with maximum porosity of 35% [6]. Lotus-type TiAl with macro cylindrical pores (in hundreds-microns scale) was fabricated by controlling the solidification rate during directional solidification in hydrogen and helium atmospheres [14,15]. This type of porous materials usually shows enhanced properties along the aligned pore direction in comparison with those porous materials with isotropic pores, which would be attractive for both structural and functional applications. Besides, the aligned pores could offer ordered channels, which may be attractive for cooling media control in active thermal protection system. Among various approaches for porous materials, freeze-casting is a novel cost-effective process to fabricate porous materials with highly aligned and elongated pores in a wide range of porosity (25%−90%) [16]. Moreover, it is also a near net shaping process which would be attractive for industrial application. The freeze-casting process normally consists of three key steps: freezing a slurry, sublimation of the frozen phase, and sintering. A unique porous structure with aligned pore channels could be obtained by unidirectional freezing the slurry. Under suitable process condition, the unidirectionally solidified crystals of liquid phase could push the particles in the slurry away from the growing path. Then, the particles accumulate among the growing crystals and the aligned pore channels can be observed after the sublimation. The pore structures at the bottom of frozen sample were usually equiaxed while the aligned and elongated pore structures can be obtained at a certain height, due to the local thermal condition change. To date, this process has been widely used to fabricate ceramics, polymers, and carbon-based materials [17−19]. However, study on this technique for porous metals is limited. A main reason should be that most engineering metal powders possess large particle size or high density in comparison with ceramic powders, leading to difficulties in preparation of stable slurries and particle redistribution. The available experiments on the fabrication of porous metals have shown the versatility of freeze-casting and indicated it would be a potential alternative to the convention processes [20−24].

In the present study, the fabrication process of porous TiAl-based intermetallics via freeze-casting was investigated. Porous TiAl materials with aligned pores were fabricated using aqueous-based slurries of commercial TiAl powders. Porous structures were tailored by freeze-casting of the slurries with different initial solid contents (10, 20 and 30 vol.%). Pore structures, compression stress and thermal conductivities were characterized with respect to aerospace thermal protection application.

2 Experimental

Engineering spherical TiAl-based intermetallic powders with average particle diameter of 50 μm (nominal composition was Ti−43Al−9V−1Y (at.%), supplied by Beijing Institute of Aeronautical Materials, China) were employed in the present work. The particle morphology and particle size distribution are shown in Fig. 1. This material belongs to γ-based TiAl intermetallics and has adequate mechanical properties from room temperature to 700 °C [25]. The particle size was measured using a laser diffraction particle size analyzer (BT−9300S, Bettersize Instruments, China). A pre-mixed solution was prepared by dissolving 1 wt.% carboxymethyl cellulose (CMC,

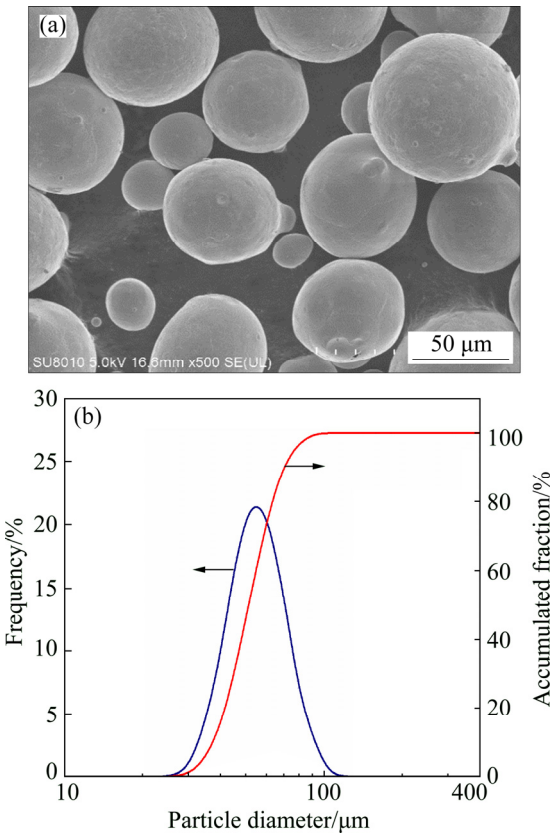

Fig. 1 SEM micrograph of raw powder (a) and particle size distribution of powder (b)

Fuchen Chemical Regent, China), and 0.6 wt.% guar gum (Guangfu Fine Chemical, China) into deionized water by stirring for 6 h. Both of CMC and guar gum act as binder and thickener to reduce sedimentation. The contents were optimized to obtain a sufficient viscosity with a low additive content. Slurries of 10, 20 and 30 vol.% particle content were prepared by adding powder into the premixed solutions under mechanical stirring for 1 h. After being stirred for 1 h, the prepared slurries were poured into cylindrical plastic molds sealed by a copper substrate. The molds were 35 mm in inner diameter and 50 mm in height and the molds were circumferential-insulated. To conduct directional freeze-casting, the filled molds were then insulated on the top and placed on a cooling plate held at −5 °C in a freeze-drier (DWBX−1, Songyuanhuaxing Ltd., China). After solidification was completed, samples were removed from the molds and freeze-dried for at least 48 h to sublimate the ice phase. The samples were subsequently placed in a vacuum furnace to carry out debinding and sintering. A slow heating rate of 2 °C/min was applied to heating the samples to 400 °C and held for 2 h to burn out the organics [21]. Then, a heating rate of 10 °C/min was applied to increasing the temperature to 1300 °C. The samples were cooled in the furnace after 2 h sintering. The main procedures of fabrication process are illustrated in Fig. 2.

The microstructure was observed by optical microscopy (OM) and scanning electron microscopy (SEM, Hitachi SU−8010, Japan). The phase compositions of the samples were identified by X-ray diffraction (XRD, Bruker D8 advanced, Germany). The porosities of the sintered sample were measured using Archimedes method. Compressive tests for loads along the aligned pores were performed in a universal material testing machine (MTS Systems, USA) at a crosshead speed of 0.5 mm/min. Test specimens are in dimensions of 10 mm × 10 mm × 15 mm. Effective thermal conductivity in room ambience was characterized by using transient hot-wire method (TC3000, Xiatech, China). All the test specimens were cut in the height range of 10−35 mm in sintered samples, in order to reduce the impact of material inhomogeneity caused by thermal condition change during unidirectional freeze.

3 Results and discussion

The longitudinal cross-section SEM morphologies of the sintered samples fabricated with different particle contents are shown in Figs. 3(a−c). It can be observed that Ti−43Al−9V−1Y particles were redistributed into elongated walls, and aligned pore channels were formed by replication of the unidirectional solidified ice crystals. The aligned pore channel could be clearly observed in typical pore morphology perpendicular to the freezing direction (Fig. 3(d)). The aligned pore structure could be attributed to the preferred growth in *a*-axis of ice crystal and the growing rate in *c*-axis lags behind [16]. The directional freezing process offered a thermal gradient from the mold substrate to the top, facilitating the directional growth of ice crystal. In fact, the local crystallization condition only allowed fine and equiaxed ice crystals to grow at the first stage of solidification, and the unidirectional crystal growth occurred after grain evolution due to freezing front velocity declining. Therefore, aligned pores could be observed above a certain height of samples.

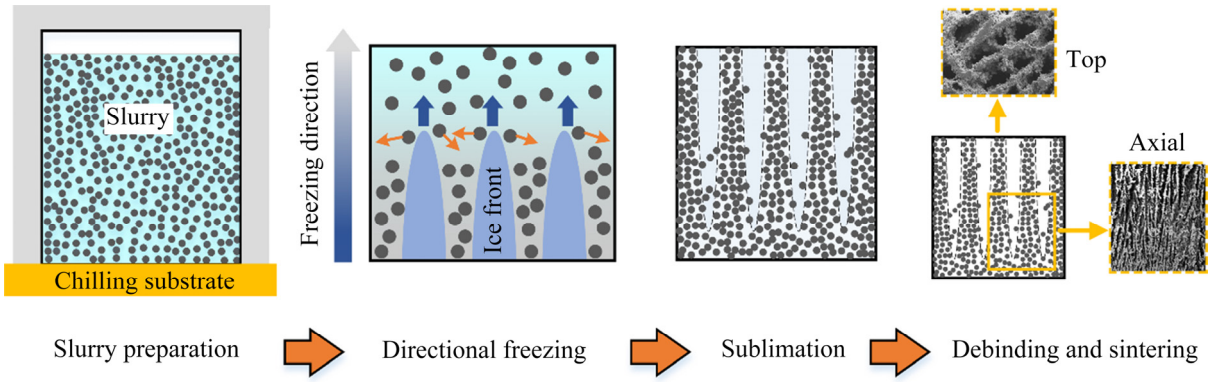

Fig. 2 Schematic of fabrication process

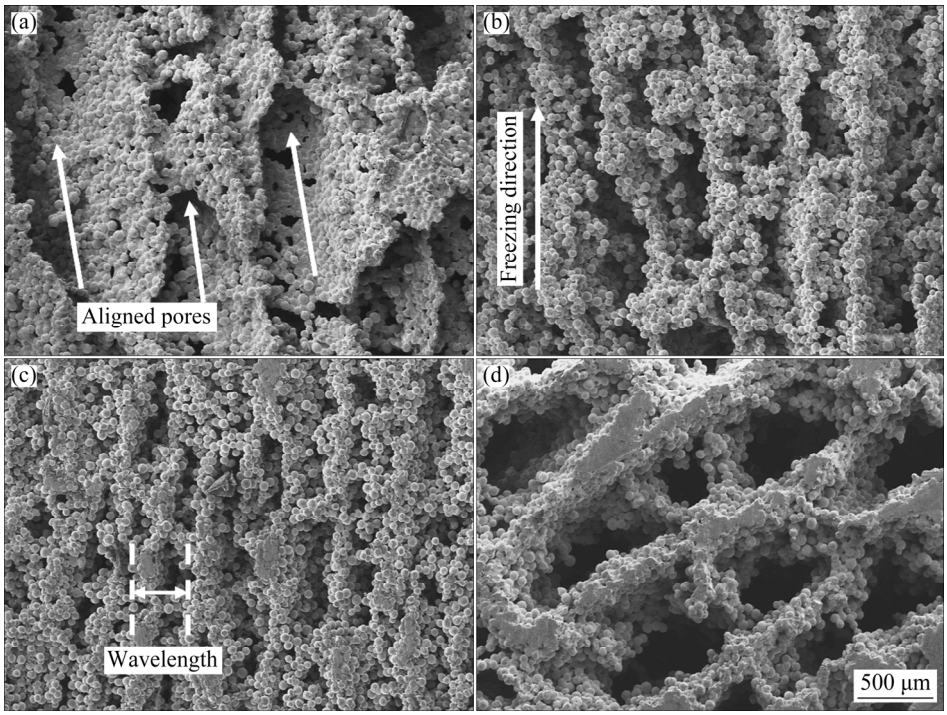

Fig. 3 SEM images of porous Ti−43Al−9V−1Y fabricated with particle contents of 10 vol. % (a), 20 vol.% (b), and 30 vol.% (c), and typical cross-section normal to freezing directions (d) (Cross-sections are parallel to freezing directions at a height of 25 mm; Wavelength denotes wall-to-wall distance or sum of aligned pore width and wall thickness)

Particle redistribution during freeze-casting is constrained by a critical freezing front velocity, v_c, which is determined according to the interaction between particle and ice front. When the freezing front growing at a velocity above the v_c, particles will be entrapped by the growing ice fronts. An adequate freezing front velocity is essential to allow the ice fronts push away the particles. An empirical model for critical freezing front velocity based on the balance of attractive forces and repulsive forces applied on particles is expressed in following equation [20]:

$$v_c = \frac{\rho_l}{9\eta\rho_s}\left[\frac{-A}{2\pi d\delta_0} - gd\delta_0(\rho_p - \rho_l)\right] \quad (1)$$

where η is the viscosity of the liquid phase, d is the particle diameter, A is the Hamaker constant of the ice−water−particle system, δ_0 is the minimal distance between the particle and freezing front, g is the gravitational constant, and ρ_l, ρ_s and ρ_p are the densities of the liquid phase, solid ice, and particle, respectively.

It can be predicted that the critical freezing front velocity decreases as the viscosity of liquid phase and particle diameter increase. For many engineering grade metal powders, the large particle size or high density leads to difficulties in particle pushing during freeze-casting. The powder used in this study has a particle size approximately an order of magnitude larger than that of ceramics widely investigated. To prevent severe sedimentation of large particles, CMC and guar gum were adopted as binder and thickener to form slurries with high viscosity. Therefore, the freezing front velocity should be low enough to allow ice crystal to push away the particles. WASCHKIES et al [26] investigated the structure formation from low (<1 μm/s) to high (>100 μm/s) freezing front velocities during freeze-casting. They studied the effects of particle size (<15 μm), solids content and freezing velocity on the microstructural evolution, and indicated that planar growth would occur when freezing front velocity was too low. In the experiment, freezing temperature was a process parameter to control the freezing process. CHEN et al [24] suggested that a lower freezing temperature applied on substrate would build up a steeper thermal gradient along the axial freezing direction. Hence, a narrow freezing period would be obtained owing to a high thermal gradient. On the contrary, a relatively high freezing temperature would lead to a long period, i.e., a low freezing

front velocity. Moreover, considering the heat transfer during freezing process as the one-dimensional heat conduction, the Fourier's law gives

$$q_z=k(T-T_s)/H \quad (2)$$

where q_z refers to heat flux in freezing direction, k is equivalent thermal conductivity, T is the temperature of slurry, T_s is the temperature of substrate, and H is the height of sample. It is indicated that q_z decreases as T_s increases when the other variables keep constant, i.e., increasing the freezing temperature would result in a low heat transfer rate through the substrate. Thus, a relatively high freezing temperature should be applied in order to obtain a low freezing front velocity along the freezing direction. In the present experiments, the freezing temperature was set as −5 °C. By measuring the freezing period of a certain frozen height, the average freezing front velocity was estimated to be 3−4 μm/s, which is relatively low in comparison with that in many studies on small ceramic particles (usually above 10 μm/s) [27−29].

Since the low freezing front velocity causes a relatively long freezing period, slurry stability should be emphasized. Particles will accumulate at the bottom and only few particles will remain at the top if sedimentation is not effectively prevented. The high local solid content at the bottom results in the failure of particles redistribution. The sedimentation during the freeze-casting was characterized by measuring the density variation from top to bottom of the test samples. Several 5 mm-long cubes were cut along the height of samples to evaluate particle sedimentation. Figure 4(a) shows that the density decreased insignificantly for each sample group prepared with 1 wt.% CMC and 0.6 wt.% guar gum in slurry. The reduction of sedimentation was facilitated, since CMC and guar gum solutions exhibited pseudoplastic rheological properties, and a CMC and guar gum mixed system could show a synergistic effect on viscosity [30]. Comparison test was also performed on slurries prepared using CMC and guar gum separately. Results showed that sedimentation could not be effectively reduced even increasing content of CMC to 3 wt.%, while unidirectional ice growth was hardly observed using slurry prepared with sufficient content of guar gum (1 wt.%). The effects of additives on slurry stability and ice crystal grow behavior still need further investigation. In the experiments, the addition of CMC and guar gum was adjusted to allow particle pushing with reduced sedimentation, as well as low additive usage.

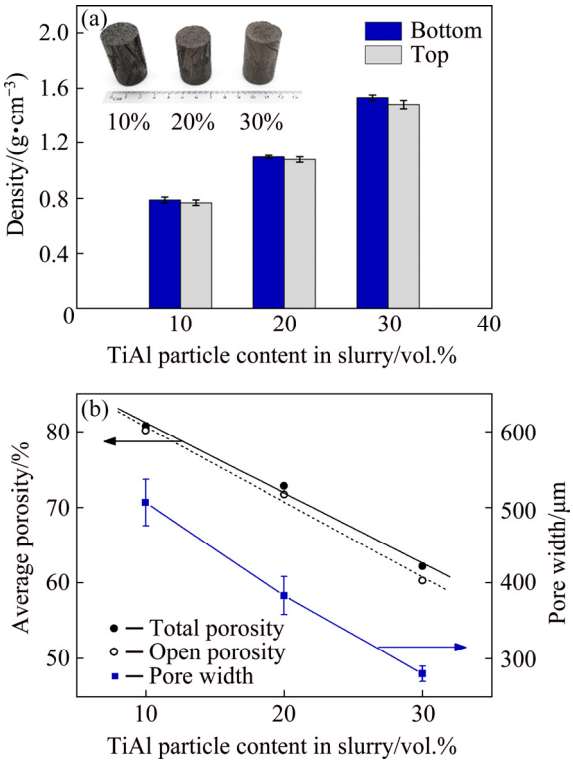

Fig. 4 Density variation of samples at bottom and top section (a) and pore properties of samples prepared with different initial TiAl particle contents (b)

It was also observed that samples prepared with different particle contents showed tuned pore morphology (Figs. 3(a−c)). The structural wavelength decreased sharply with increasing the particle content. As shown in Fig. 4(b), with particle content rising from 10 to 30 vol.%, the aligned pore width decreased from (500±30) to (270±20) μm. This decrease trend could be attributed to the rise of ice front velocity which was induced by the increase in the particle content [28,29]. An empirical relationship between wavelength and freezing front velocity was given by [28]

$$\lambda \propto 1/v^n \quad (3)$$

where λ is the wavelength, v is the freezing front velocity, and n could be regarded as a variable depending on particle size, volume fraction, temperature gradient, and other complex factors during the process. The pore structures of the

products were found to be hierarchical. Besides the aligned pores formed by replication of ice crystals, second order isotropic pores were found among the spherical particles located in channel wall, particularly in samples prepared with 10 and 20 vol.% particle content. These pores connected the aligned pores and further increased the porosity, as shown in Fig. 5. The fabricated materials exhibited favorable porosities and high open porosity percentage (above 90%) than porous TiAl with aligned pores [6,15]. According to Fig. 3(b), total porosity could be controlled in the range from 62% to 81% by varying particle content. It can be expected that porosity and aligned pore structure could be tailored by particle content or other processing parameters.

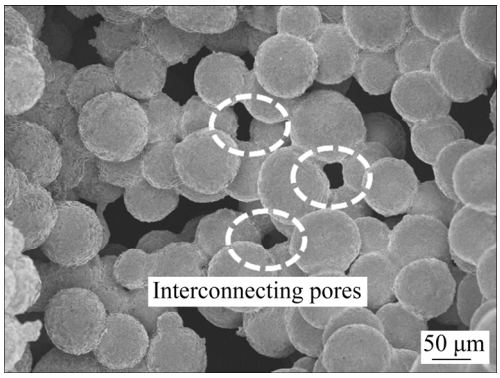

Fig. 5 SEM image of typical interconnecting pores

The evolution of pore structure at different heights in the samples is shown in Fig. 6. The pore channels exhibited a columnar-to-lamellar transition structure as aligned pores extended from the bottom of the samples, due to the change of freezing condition. This pore structure evolution was consistent with the decrease in freezing front velocity. DEVILLE et al [28] found that the ice dendrite tip radius increased as the freezing front velocity decreased owing to the reduction in undercooling ahead of the solid/liquid interface. Thus, the ice crystals were coarsened and the pore width increased. CHINO and DUNAND [20] showed that the freezing front velocity was not affected by the powder size and it decreased monotonously with increasing frozen height. The decrease of freezing front velocity was attributed to the much lower thermal conductivity of solidified slurry as compared to copper substrate and the increased frozen height. Theoretically, a constant freezing front velocity could be achieved by optimizing freezing conditions [31], and thus the precision control of the microstructure could be achieved for this process.

Figure 7 shows the typical XRD pattern of sintered Ti−43Al−9V−1Y. The major γ phase and a small amount of α_2 and B_2 phases were clearly identified, which was consistent with previous studies [25,32,33]. The addition of Y was initially designed to protect the material from oxidization since Y has stronger binding capability with O, and oxides were hardly to be detected, indicating that

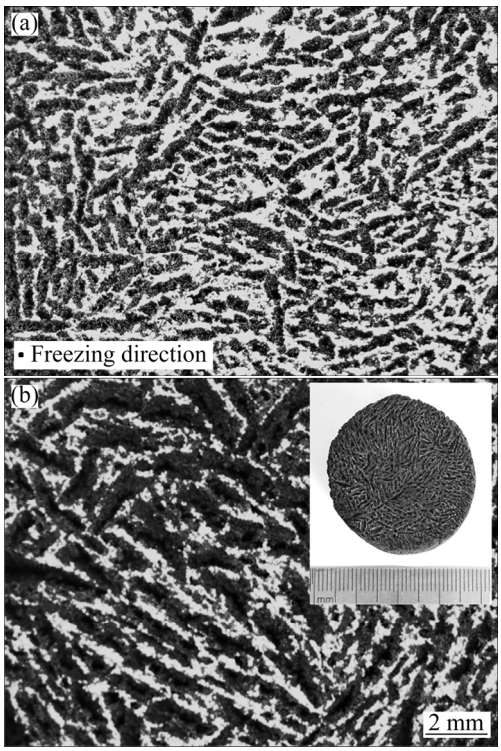

Fig. 6 OM micrographs of cross-sections perpendicular to freezing direction at different heights with 30 vol.% particle content: (a) 10 mm; (b) 35 mm

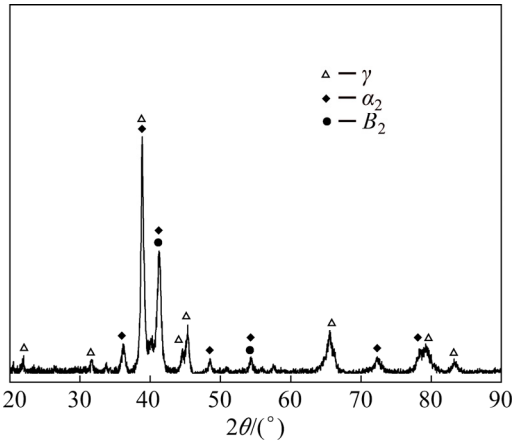

Fig. 7 XRD pattern of porous Ti−43Al−9V−1Y fabricated with 30 vol.% particle content

porous Ti−43Al−9V−1Y materials could be fabricated via this process without notable oxidization.

Table 1 shows typical literature data of porosity and pore size for TiAl-based porous material and data achieved in this study. It can be seen that a high level of porosity was achieved in this work, indicating a great potential to produce porous TiAl by this process. Moreover, the TiAl samples prepared by freezing-casting had unique aligned pores. Compared to other fabrication processes for unidirectional pores, freeze-casting could offer higher porosity and larger pore size range. Previous research indicates that open-cell porous metals are usually suitable for functional applications, rather than use as structure component. However, there is growing demand for special porous metals that possess light weight, high porosity, heat insulation function, as well as load-bearing capability in aerospace engineering [38]. For instance, an aerospace thermal protection plate is designed with a sandwich structure and requires a good compression load resistance in vertical axial [39]. The freeze-cast TiAl foam could be used as insulation material filled in the place between the face sheets to insulate against heat and bear a part of compression load.

The mechanical performance of the freeze-cast porous TiAl was characterized by compressive strain−stress test along aligned pore direction, since this direction was considered to have superior strength to support the heat protection structure. In general, the mechanical strength of porous materials largely relies on the porosity and the pore structure. For most porous materials, higher porosity leads to lower mechanical strength. However, a higher porosity can provide more cavities for air in the porous material and decrease the heat conduction when the porous material is used in thermal insulation application. Therefore, the porosity and the mechanical performance should be traded off in order to offer a favorable thermal protection performance, as well as to maintain good structural integrity during service of the porous materials. Figure 8 shows the compressive properties varied with particle content. Compressive strength along aligned pore increased sharply from 16 to 120 MPa when the particle content increased from 10 to 30 vol.%. This should be attributed to the increased solid content and the pore wall densification. It was found that the fabricated materials demonstrated a superior compressive performance in aligned direction to a type of porous TiAl with homogenous pores [10].

Table 1 Literature and measured values of open porosity, pore size and pore structure for porous TiAl-based intermetallics prepared via different processes

Process	Open porosity/ %	Pore size/ μm	Pore structure	Source
Reactive sintering	25−45	−	Aligned	[6,34]
Unidirectional solidification	15−56	~470	Aligned	[14,15]
EPM	<52	3.18−26.69	Isotropic	[5,8]
PM	~70	~30	Isotropic	[35]
Reactive infiltration	< 70	~100	Isotropic	[36]
TE with space holder	72−84	50−500	Hierarchical	[37]
Freeze casting	62−81	270−500	Aligned	This study

EPM—Element powder metallurgy; PM—Powder metallurgy; TE—Thermal explosion

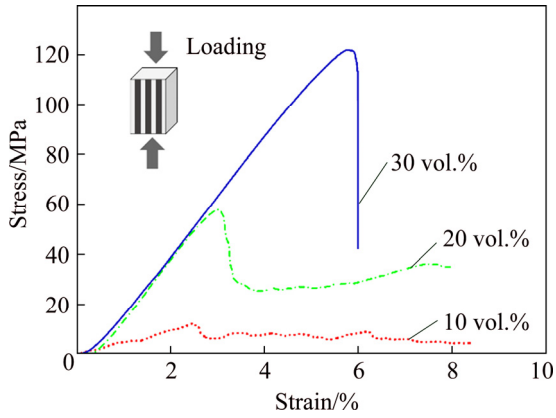

Fig. 8 Compressive stress−strain curves for porous materials fabricated with particle contents of 10, 20 and 30 vol.% (Loads are parallel to the pore orientations)

Effective thermal conductivities of the porous materials (k_e) were analyzed with the Maxwell−Eucken models [13]:

$$k_e = k_s \frac{2k_s + k_g - 2(k_s - k_g)P}{2k_s + k_g + (k_s - k_g)P} \quad \text{(Maxwell−Eucken 1)} \tag{4}$$

$$k_e = k_g \frac{2k_g + k_s - 2(k_g - k_s)(1-P)}{2k_g + k_s + (k_g - k_s)(1-P)} \quad \text{(Maxwell−Eucken 2)} \tag{5}$$

where k is the effective thermal conductivity, P is the total porosity, and subscripts "e", "s" and "g" refer to the hybrid system, Ti−43Al−9V−1Y and air, respectively. Thermal conductivity for bulk Ti−43Al−9V−1Y was estimated to be 36.0 W/(m·K), according to the calculation of JMatPro commercial software. The measured values and the model curves are shown in Fig. 9. The experiment results were in the predicted region and closer to the lower boundary. This result could be attributed to the overestimated thermal conductivity for bulk Ti−43Al−9V−1Y or other factors related to porous structures. It was observed that k_e exhibited anisotropic property and decreased as the total porosity increased. For a fixed porosity, the effective thermal conductivity parallel to the unidirectional pore orientation ($k_{parallel}$) was larger than that perpendicular to the pore orientation ($k_{perpendicular}$). An average anisotropic factor in thermal conductivity ($k_{parallel}/k_{perpendicular}$) was estimated to be around 1.4. The maximum thermal conductivity was only 1.81 W/(m·K), showing an excellent potential for lightweight metallic thermal insulators [7]. It was found that the fabricated materials also demonstrated a competitive mechanical and thermal insulating property in comparison with porous ceramics [40,41]. Such a combination of strength and heat insulation performance makes the porous TiAl an attractive choice for aerospace thermal protection.

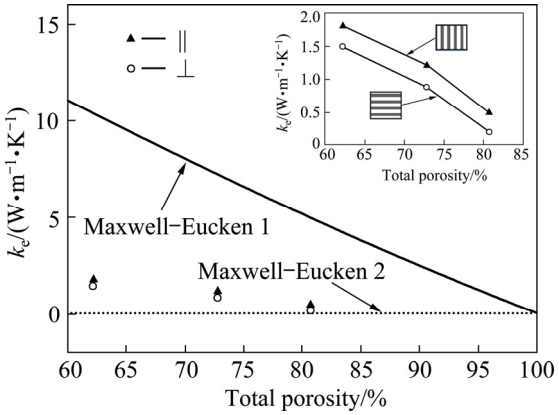

Fig. 9 Effective thermal conductivities for porous materials (Each data point represents an average of three tests)

4 Conclusions

(1) Porous Ti−43Al−9V−1Y materials with aligned and elongated pores were fabricated by freeze-casting. The spherical particles as large as 50 μm in CMC and guar gum aqueous slurries could be redistributed into the interlamellar spaces with applying a relatively high freezing temperature of −5 °C.

(2) The porosity was tailored by varying the particle content in the slurry from 10 to 30 vol.%. With increasing the particle content from 10 to 30 vol.%, the total porosity reduced from 81% to 62% and the aligned pore width dropped from approximately 500 to around 270 μm.

(3) The increase of particle content led to an increase of compressive strength along the aligned pores (from 16 to 120 MPa). The effective thermal conductivity of porous TiAl increased as the particle content increased (lower than 1.81 W/(m·K)) and showed anisotropic property with respect to the pore orientation.

References

[1] WU Xin-hua. Review of alloy and process development of TiAl alloys [J]. Intermetallics, 2006, 14: 1114−1122.

[2] ISMAEEL A, WANG Cun-shan. Effect of Nb additions on microstructure and properties of γ-TiAl based alloys fabricated by selective laser melting [J]. Transactions of Nonferrous Metals Society of China, 2019, 29: 1007−1016.

[3] ZHAO Kun, OUYANG Si-hui, LIU Yong, LIU Bin, LIANG Xiao-peng, LI Hui-zhong, WANG Yu. Isothermal oxidation behavior of TiAl intermetallics with different oxygen contents [J]. Transactions of Nonferrous Metals Society of China, 2019, 29: 526−533.

[4] CHEN Huan-ming, LI Xiao-wei, CHEN Zhi-peng, ZHANG Rui, MA Xiao-bo, ZHENG Fu, MA Zhi, PAN Feng-chun, LIN Xue-ling. Investigation on electronic structures and mechanical properties of Nb-doped $TiAl_2$ intermetallic compound [J]. Journal of Alloys and Compounds, 780: 41−48.

[5] YANG Fan, ZHANG Lai-qi, LIN Jun-pin, LIANG Yong-feng, HE Yue-hui, SHANG Shun-li, LIU Zi-kui. Pore structure and gas permeability of high Nb-containing TiAl porous alloys by elemental powder metallurgy for microfiltration application [J]. Intermetallics, 2013, 33: 2−7.

[6] YANG S H, KIM W Y, KIM M S. Fabrication of unidirectional porous TiAl−Mn intermetallic compounds by reactive sintering using extruded powder mixtures [J]. Intermetallics, 2003, 11: 849−855.

[7] WANG Y H, LIN J P, HE Y H, ZU C K, CHEN G L. Pore structures and thermal insulating properties of high Nb containing TiAl porous alloys [J]. Journal of Alloys and Compounds, 2010, 492: 213−218.

[8] LIANG Yong-feng, YANG Fan, ZHANG Lai-qi, LIN Jun-pin, SHANG Shun-li, LIU Zi-kui. Reaction behavior and pore formation mechanism of TiAl−Nb porous alloys prepared by elemental powder metallurgy [J]. Intermetallics,

2014, 44: 1−7.

[9] JIANG Y, HE Y H, XU N P, ZOU J, HUANG B Y, LIU C T. Effects of the Al content on pore structures of porous Ti−Al alloys [J]. Intermetallics, 2008, 16: 327−332.

[10] HAO Gang-ling, WANG Hui, LI Xian-yu. Novel double pore structures of TiAl produced by powder metallurgy processing [J]. Materials Letters, 2015, 142: 11−14.

[11] KOBASHI M, MIYAKE S, KANETAKE N. Hierarchical open cellular porous TiAl manufactured by space holder process [J]. Intermetallics, 2013, 42: 32−34.

[12] JIAO Xin-yang, WANG Xiao-hong, KANG Xue-qin, FENG Pei-zhong, ZHANG Lai-qi, AKHTAR F. Effect of heating rate on porous TiAl-based intermetallics synthesized by thermal explosion [J]. Materials and Manufacturing Processes, 2017, 32: 489−494.

[13] DU H, LIU X W, LI J, TAO P, JIANG J, SUN R, FAN Z T. Use of spark plasma sintering for fabrication of porous titanium aluminide alloys from elemental powders [J]. Materials and Manufacturing Processes, 2016, 31: 725−732.

[14] IDE T, TANE M, NAKAJIMA H. Compressive deformation behavior of porous γ-TiAl with directional pores [J]. Materials Science and Engineering A, 2009, 508: 220−225.

[15] YANG F, TANE M, LIN J P, SONG Y H, NAKAJIMA H. Pore formation and compressive deformation in porous TiAl−Nb alloys containing directional pores [J]. Materials and Design, 2013, 49: 755−760.

[16] DEVILLE S. Freeze-casting of porous ceramics: A review of current achievements and issues [J]. Advanced Engineering Materials, 2008, 10: 155−169.

[17] SCOTTI K L, DUNAND D C. Freeze casting—A review of processing, microstructure and properties via the open data repository, FreezeCasting.net [J]. Progress in Materials Science, 2018, 94: 243−305.

[18] CAO Ji-wei, LU Zhong-liang, MIAO Kai, ZHAO Hong-jiong, XIA Yuan-lin, WANG Fu, LU Bing-heng. Fabrication of high-strength porous SiC-based composites with unidirectional channels [J]. Journal of the American Ceramic Society, 2019, 102: 4888−4898.

[19] SIVASHANKARI P R, MOORTHI A, MOHAMED A K, PRABAHARAN M. Preparation and characterization of three-dimensional scaffolds based on hydroxypropyl chitosan-graft-graphene oxide [J]. International Journal of Biological Macromolecules, 2018, 110: 522−530.

[20] CHINO Y, DUNAND D C. Directionally freeze-cast titanium foam with aligned, elongated pores [J]. Acta Materialia, 2008, 56: 105−113.

[21] WEAVER J S, KALIDINDI S R, WEGST U G K. Structure-processing correlations and mechanical properties in freeze-cast Ti−6Al−4V with highly aligned porosity and a lightweight Ti−6Al−4V-PMMA composite with excellent energy absorption capability [J]. Acta Materialia, 2017, 132: 182−192.

[22] LIU Xin-li, WU Ji-si, LUO Bo, ZHANG Lei, LAI Yan-qing. Porous Cu foams with oriented pore structure by freeze casting [J]. Materials Letters, 2017, 205: 249−252.

[23] DEVILLE S. The lure of ice-templating: Recent trends and opportunities for porous materials [J]. Scripta Materialia, 2018, 147: 119−124.

[24] CHEN Huan-ming, MA Ya-nan, LIN Xin-xin, YANG Dong, CHEN Zhi-peng, LI Xiao-wei, LIN Xue-ling, PAN Feng-chun, MA Zhi. Preparation of aligned porous niobium scaffold and the optimal control of freeze-drying process [J]. Ceramics International, 2018, 44: 17174−17179.

[25] LI B H, CHEN Y Y, HOU Z Q, KONG F T. Microstructure and mechanical properties of as-cast Ti−43Al−9V−0.3Y alloy [J]. Journal of Alloys and Compounds, 2009, 473: 123−126.

[26] WASCHKIES T, OBERACKER R, HOFFMANN M J. Investigation of structure formation during freeze-casting from very slow to very fast solidification velocities [J]. Acta Materialia, 2011, 59: 5135−5145.

[27] GHOSH D, KANG H, BANDA M, KAMAHA V. Influence of anisotropic grains (platelets) on the microstructure and uniaxial compressive response of ice-templated sintered alumina scaffolds [J]. Acta Materialia, 2017, 125: 1−14.

[28] DEVILLE S, SAIZ E, TOMSIA A P. Ice-templated porous alumina structures [J]. Acta Materialia, 2007, 55: 1965−1974.

[29] PREISS A, SU B, COLLINS S, SIMPSON D. Tailored graded pore structure in zirconia toughened alumina ceramics using double-side cooling freeze casting [J]. Journal of the European Ceramic Society, 2012, 32: 1575−1583.

[30] HAYATI I N, CHING C W, ROZAINI M Z H. Flow properties of O/W emulsions as affected by xanthan gum, guar gum and carboxymethyl cellulose interactions studied by a mixture regression modelling [J]. Food Hydrocolloids, 2016, 53: 199−208.

[31] WASCHKIES T, OBERACKER R, HOFFMANN M J. Control of lamellae spacing during freeze casting of ceramics using double-side cooling as a novel processing route [J]. Journal of the American Ceramic Society, 2009, 92: 79−84.

[32] CHEN Yu-yong, KONG Fan-tao, HAN Jie-cai, CHEN Zi-yong, TIAN Jing. Influence of yttrium on microstructure, mechanical properties and deformability of Ti−43Al−9V alloy [J]. Intermetallics, 2005, 13: 263−266.

[33] CHEN Rui-run, ZHAO Xiao-ye, YANG Yong, GUO Jing-jie, DING Hong-sheng, SU Yan-qing, FU Heng-zhi. Effect of Zr on microstructure and mechanical properties of binary TiAl alloys [J]. Transactions of Nonferrous Metals Society of China, 2018, 28: 1724−1734.

[34] KIM J M, KIM J, YOON S H, HYUN S K, KIM M S. Fabrication and compressive properties of porous TiAl−Mn intermetallics by powder metallurgical route [J]. Metals and Materials International, 2013, 19: 159−162.

[35] PENG Qin, YANG Bin, LIU Li-bin, SONG Chang-jiang, FRIEDRICH B. Porous TiAl alloys fabricated by sintering of TiH_2 and Al powder mixtures [J]. Journal of Alloys and Compounds, 2016, 656: 530−538.

[36] ZHANG W, LIU Y, WANG H, WEI Q Q. Preparation and properties of porous Ti−Al alloys by reactive infiltration [J]. Powder Metallurgy, 2011, 54(3): 253−256.

[37] WANG Zhang, JIAO Xin-yang, FENG Pei-zhong, WANG Xiao-hong, LIU Zhang-sheng, AKHTAR F. Highly porous open cellular TiAl-based intermetallics fabricated by thermal explosion with space holder process [J]. Intermetallics, 2016, 68: 95−100.

[38] ZHU Chun-sheng, GUO Ce, DAI Zheng-dong. Fabrication

and study of porous metals with a highly regular structure [J]. Materials Letters, 2013, 94: 189−192.

[39] FANG Xue-wei, CHEN Jian, LU Bing-heng, WANG Yi-qing, GUO Shan-guang, FENG Zheng-yi, XU Ming-long. Optimized design of sandwich panels for integral thermal protection systems [J]. Structural and Multidisciplinary Optimization, 2017, 55: 13−23.

[40] ZHANG Ru-bing, FANG Dai-ning, CHEN Xiang-meng, PEI Yong-mao, WANG Zheng-dao, WANG Yue-sheng. Microstructure and properties of highly porous Y_2SiO_5 ceramics produced by a new water-based freeze casting [J]. Materials and Design, 2013, 46: 746−750.

[41] GONG Lun-lun, WANG Yong-hong, CHENG Xu-dong, ZHANG Rui-fang, ZHANG He-ping. Thermal conductivity of highly porous mullite materials [J]. International Journal of Heat and Mass Transfer, 2013, 67: 253−259.

冷冻浇注制备多孔钛铝基金属间化合物的显微组织及性能

鲁中良[1,2,3]，徐文梁[1]，曹继伟[1]，夏园林[1]，邓清华[4]，李涤尘[1]

1. 西安交通大学 机械工程学院 机械制造系统工程国家重点实验室，西安 710049；
2. 沈阳铸造研究所 高端装备轻合金铸造技术国家重点实验室，沈阳 110022；
3. 先进航空发动机协同创新中心，北京 100191；
4. 西安交通大学 能源与动力工程学院，西安 710049

摘 要：通过冷冻浇注法制备具有定向长孔结构的多孔钛铝基金属间化合物。采用 Ti−43Al−9V−1Y 工程级粉末(D_{50}=50 μm)、羧甲基纤维素以及瓜尔豆胶配制水基浆料用于冷冻浇注。研究结果表明，在−5 °C 的冷冻条件下可制备具有定向长孔结构的多孔钛铝，并且可通过改变浆料中粉末的体积分数来控制孔隙结构。当粉末含量从 10%增加至 30% (体积分数)时，总孔隙率由 81%减小至 62%，定向孔宽度由约 500 μm 减小至约 270 μm。随着孔隙率的降低，沿定向孔方向的压缩强度由 16 MPa 增加至 120 MPa。另外，所制备的多孔钛铝的等效热导率较低，最高为 1.81 W/(m·K)，并且受孔方向的影响呈现出各向异性。

关键词：多孔 TiAl；冷冻浇注；孔隙结构；力学性能；热导率

(Edited by Bing YANG)